Empirical models of mechanical behaviour of Al-Si-Mg cast alloys for high performance engine applications

Andrea Morri
SMETEC Dept., University of Bologna, Bologna, Italy

Winner of Daccò Prize 2010
competition promoted by AIM - Italian Association of Metallurgy

ABSTRACT

The main limitation of cast Al-Si-Mg alloys is the considerable influence of the solidification and heat treatment conditions on the final microstructure and consequently on the mechanical properties, that can thus widely vary in the same cast component. In this work we perform a deep microstructural and mechanical characterisation on specimens extracted from some A356 T6 gravity die cast cylinder heads. The aim of the work is to develop empirical models to successfully predict the local tensile properties of the casting from the main microstructural parameters and alloy hardness. As the former we considered and measured secondary dendrite arm spacing, shape and size of the eutectic silicon, grain size and percentage area of defects. The latter instead primarily depends on the heat treatment conditions. On the base of these data we propose a set of simple equations to predict the ultimate tensile strength and the proof strength with a mean error of 2% and the elongation to failure with a mean error of 20%. The equations allow the designer to know the local tensile behaviour without any tensile tests. Moreover, in a co-engineered design approach, the equations can link the post-processing results of the casting simulation software to the pre-processing phase of the structural software. This leads to less bench tests and to a great reduction of validation time of a new product.

RIASSUNTO

Il maggiore limite dei getti in lega Al-Si-Mg risiede nella elevata influenza delle condizioni di solidificazione e del trattamento termico sulla miscrostruttura finale e, di conseguenza, sulle proprietà meccaniche che possono dunque variare notevolmente nello stesso getto. In questo lavoro è stata condotta un'approfondita caratterizzazione microstrutturale e meccanica di provini ricavati da teste motore, in lega di alluminio A356 T6, ottenute mediante colata in conchiglia. L'obiettivo della ricerca è stato quello di mettere a punto modelli previsionali delle principali proprietà tensili della lega, sulla base dei principali parametri microstrutturali e dei valori di durezza. Fra i primi sono stati misurati: dimensione del grano, spaziatura tra i rami secondari dendritici (SDAS), forma e dimensione media del Si eutettico ed area percentuale dei difetti di solidificazione. La seconda dipende invece in prima misura dall'efficacia del trattamento termico. Sulla base di questi dati, vengono proposti modelli empirici per predire la resistenza a snervamento e trazione con un errore del 2% e l'allungamento a rottura con un errore medio del 20%. Le equazioni consentono al progettista la valutazione delle proprietà meccaniche locali del materiale senza bisogno di eseguire alcun test di trazione. Inoltre, nel caso di una progettazione di tipo integrato, tali equazioni possono rappresentare l'anello di giunzione tra le fasi di post-processing dei software di simulazione di processo e di pre-processing dei software di simulazione strutturale, portando ad una notevole riduzione dei test a banco e del tempo di validazione dei nuovi motori.

KEYWORDS

356, mechanical properties, microstructures, hardness, models.

Acronyms. optical microscopy: OM; scanning electron microscopy: SEM; Transmission electron microscopy: TEM; Image analysis: IA; Grain size (d); Secondary dendrite arm spacing: SDAS; Aaspect ratio of eutectic silicon particles: AR; Area of eutectic silicon particles: A; Percentage area fraction of solidification defects: AF%; percentage cross section: CS% =100-AF%; Brinell hardness: HB; Ultimate tensile strength: UTS; 0.2% proof strength: YS; elongation to failure: E%;

INTRODUCTION

Excellent castability, corrosion resistance and high strength-to-weight ratio (which increases performance and fuel economy) have made cast Al–Si–Mg alloys suitable candidate materials for various applications in the automotive industry, such as engine blocks and cylinder heads. With these alloys (typically A356 and A357) it is possible to cast complex and thin-walled components through either sand, die and permanent mould casting with tensile strengths up to 350 MPa [1-3]. This high strength level is achieved through the T6 heat treatment. In particular Mg–Si precipitates provide strengthening through age hardening. The main limitations of Al-Si-Mg cast components are due to the considerable influence of the solidification conditions on the final microstructure. The final cast component inevitably contains a certain number of defects such as oxide films, shrinkage and gas porosity, which significantly affect the mechanical properties and in particular the fatigue behaviour [4-6]. As reported in [6], the fatigue life of cast alloys containing defects can be one or two orders of magnitude shorter than for defect-free cast components. The static mechanical properties are not as much influenced as fatigue by solidification defects, but can be more affected by others microstructural parameters [7-13]. The microstructure of A356/357 casting alloys is composed of primary aluminium dendrites, eutectic silicon and Fe-rich particles. The volume fraction of dendrites and eutectic particles is determined by chemistry, whereas their size and distribution are mainly dominated by solidification conditions. For a given alloy, the α-Al matrix and the eutectic silicon morphology can also be affected by the heat treatment. Therefore, the size, volume and morphology of microstructural constituents are functions of chemistry, solidification conditions and heat treatment. The static mechanical properties are mainly affected by SDAS and by the size and distribution of the second phase particles [9-13]. It is in fact widely reported that the tensile failure of Al–Si–Mg alloys occurs in three stages: (1) cracking of the eutectic silicon particle at low plastic strains (1–2%); (2) generation of localised shear bands with microcracks forming from the joining of adjacent cracked particles; (3) microcracks coalescence followed by propagation, leading to the final fracture. All these issues must be considered during the design of complex Al-Si-Mg cast components as a variety of local microstructures in the casting can lead to different mechanical properties. Most of the literature concerns the relationships between the solidification microstructure and mechanical properties as obtained by specimens produced under controlled laboratory conditions [4-12]. The cylinder heads we used in this study were produced through gravity die casting using the A356 aluminium alloy and were industrially heat treated at the T6 condition. In this work we first aimed at obtaining a map of the main microstructural parameters of the described cylinder head; second, we aimed at measuring the local mechanical properties using specimens directly machined from the cast; finally we found mathematical models to predict the local tensile properties of the casting knowing the main microstructural parameters and alloy hardness. The models allow the designer to predict the local tensile properties even in parts of the cast where the extraction of specimens is not possible. Moreover, in the case of a co-engineering design approach with intensive and reliable use of casting simulation software, the proposed predictive models can return the local mechanical properties of the cast that can be given as input to the structural simulation software. This leads to less bench tests and to a great reduction of validation time of a new product.

EXPERIMENTAL

THE CYLINDER HEAD

A primary A356 aluminium alloy (EN AC 42100) is used to fabricate cylinder heads (Fig. 1a) through gravity die casting. The chemical composition of the alloy, as obtained by spectrometric analyses, is listed in Tab. 1.

The A356 ingots are first remelted in a gas furnace. The hydrogen level in the melt is reduced by using a rotary lance degasser and a high purity argon gas. Grain refinement and eutectic Si modification are achieved by adding, during the degassing process, commercial Al-Ti-B (Al-5%Ti-1%B) and Al-10wt.%Sr master alloys, respectively. The level of hydrogen is controlled by verifying that, after the degassing operation, density don't exceed the lower limit of 2.64 Kg/dm^3. Chemical composition of the melt was controlled through spectrometric analyses.

The melt is then poured into a maintenance furnace at 730°C and then poured into the mould. Solidification of the cast occurs in about 20s since the end of the filling. After 9 minutes, the die is opened. The first step of the sand handling consists of high temperature exposure (500°C) and shakeout operations. The casting system is then removed and the cast is brought to the T6 condition through solution (535°C for 4.5h), water quenching (20-60°C) and aging (165°C for 4.5h). The time between solution and aging treatments ("*pre-aging*") during which castings remain at room temperature can range between 0 and 2h. If any problem in the managing of the furnaces occurs so that a longer pre-aging time might be reached, the castings are stored at -30°C. Brinell hardness tests are carried out on the whole production, on fixed points of the castings to verify the effect of the heat treatment. Target values ranging between 95 and 105 HB.

The experimental analysis was carried out by extracting samples and specimens from three cylinder heads in the T6 conditions and one in the as-cast conditions.

Table 1. Chemical composition of the A356 Al alloy (weight %)

Si	Mg	Fe	Cu	Mn	Zn	Ti	Sr	B	Al
7.24	0.42	0.138	<0.001	0.007	0.003	0.120	0.015	0.0354	Bal.

MECHANICAL TESTING

50 specimens for mechanical testing were cut from different parts (Fig. 1b) of the cylinder head in the as-cast condition. Before the machining of the samples, the previously mentioned heat treatment was performed. Different set of specimens were obtained, one for each different pre-aging time (between 0 and 2h). Mechanical characterisation of the heat treated specimens was performed through (1)

Brinell hardness tests (HBW 2.5/62.5) according to the ASTM E 10–08 standard [14] and (2) tensile tests according to the UNI EN 10002-1:2004 standard [15]. Tensile tests were performed on a screw testing machine at room temperature with a nominal strain rate of $3.3 \cdot 10^{-3} s^{-1}$, and using 50 flat specimens (Fig. 1c) with a gauge length L_o=30mm and a cross-sectional area S_o=25mm^2. We tested 6 specimens for each pre-aging condition to evaluate the 0.2% proof strength, the ultimate tensile strength and the elongation to failure.

MICROSTRUCTURAL ANALYSIS

We performed OM microstructural analysis on sections of the heat treated cylinder head (Fig. 1d) and on a cross section near to the fracture surface of the tensile specimens. Metallographic specimens were prepared using standard metallographic techniques including mechanical grinding and polishing with 9 μm and 1 μm diamond paste (according to the ASTM E3 [16]). We revealed the grain structure using electrolytic etching with Barker's reagent (5ml HBF_4 (50%wt.), 100ml distilled water) and anodising for 80s at 15V (according to ASTM E 883 standard [17]). We performed IA in order to measure grain size, SDAS, aspect ratio and area of the eutectic silicon particles. We evaluated these microstructural parameters by considering about 30 optical micrographs for each tensile specimen and about 2000 micrographs for each analysed section of the casting. Such a high number of micrographs was necessary due to the wide surface (about 1 dm^2) of the sections. The grain size was measured on the electrolytically etched samples observed under polarised light, according to the Heyn Linear Intercept Procedure described in the ASTM E112 standard [18]. We measured the value of SDAS by identifying and measuring aligned groups of secondary cells. The value of SDAS was then calculated as *SDAS=L/n*, where *L* is the length of the line drawn from edge to edge of the measured cells and *n* the number of the dendrite cells. At least 100 cells for each sample were considered. Aspect ratio and area of the eutectic Si particles was evaluated as the ratio of major and minor axes of the equivalent ellipse on about 2000 particles for each sample. This number of particle was that one identified as consistent by some previous analisys. It was obtained by considering about 20 high magnification micrographs for each specimen (corresponding to about 1% of its cross section).

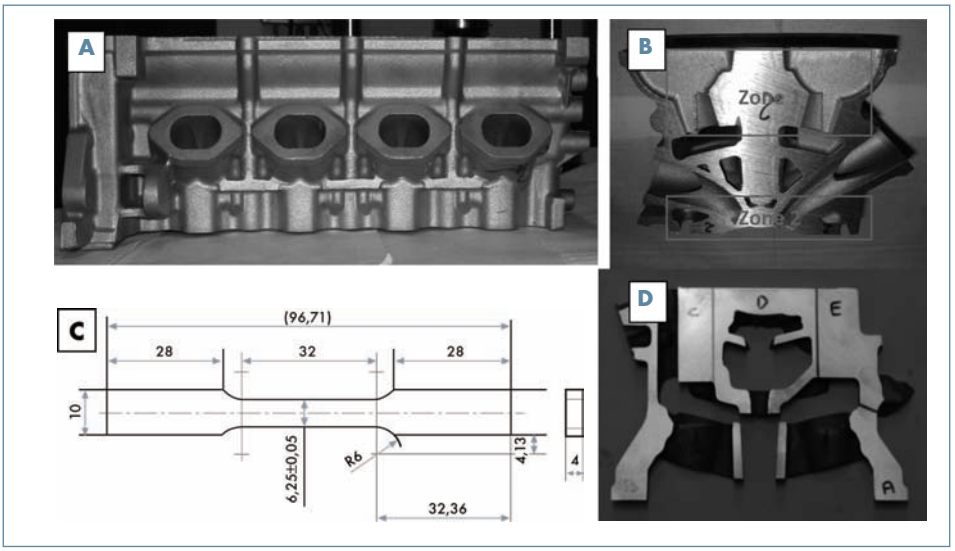

Fig. 1: The cylinder head (a); examples of zones of extraction of tensile test specimens (b); dimensions of tensile test specimens (c); a section of the casting used for microstructural characterization.

We used a Zeiss Evo®50 scanning electron microscope to analyse the fracture surfaces of the tensile specimens. The percentage area fraction of the solidification defects (such as gas pores and cavity shrinkages) on the fracture surfaces was evaluated by image analyses. The actual cross section of the tensile specimens was estimated as CS% = 100 – AF%. For this evaluation, the total area of defects measured on the fracture surface was divided by the nominal cross section of the specimen (measured with a micrometer before the tensile test). This choice can be explained by considering that: 1) IA on a single random metallographic section of the specimen cannot give a true evaluation of the defects content; 2) it is highly probable that the fracture surface of the specimen is the one with the highest defects content. IA of OM and SEM micrographs was performed with the *Image pro-Plus*® software.

CORRELATION ANALYSIS

We first used a correlation matrix [19] to define the correlations among mechanical properties and microstructural parameters. Given a nxn correlation matrix A, where n is the total number of considered mechanical properties and microstructural parameters, each element A[i,j] represents the Pearson's correlation coefficient between property/parameter i and property/parameter j (in the range [-1;1]). In particular the higher is the absolute value of the coefficient, the higher the correlation between the properties/parameters. Once the parameters with highest correlation with the mechanical properties were identified, their relationships with the mechanical properties were evaluated using multiple variable regression analysis (performed with the *XLstat*® software).

RESULTS AND DISCUSSION

MECHANICAL TESTING

Hardness tests on the tensile specimens have shown the effect of pre-aging on the alloy hardness after the T6 heat treatment. Tab. 2 shows the results of the tests. As also reported in [20], it is clear how longer pre-aging time results into a less hard final alloy. Considering the case where no pre-aging occurs as ideal situation, in our experiments the hardness loss was about 15 HB for pre-ageing time of 60 min. Pre-aging time longer than 60 min., on the other hand, did not have any further significant effect on the alloy hardness.

The results of the tensile tests showed that the pre-aging time variation led to a similar effect on the 0,2% proof strength and ultimate tensile strength. A decrease of about 50 MPa occurs with 60 min. of pre-aging time for both the tensile properties. On the other hand, the maximum values of elongation to failure of the different sets of specimens seem to increase with the pre-aging time. The effect of the pre-aging on the minimum values of elongation to failure seems instead negligible. Considering both the minimum and maximum values of E%, it seems clear that the higher is the pre-aging time, the larger the scatter in the data. By increasing the pre-aging time, we obtained a great reduction in the alloy hardness but a non systematic elongation to failure increase. The hardness (pre-aging time) could not so be considered the unique parameter we have to consider in the

tensile properties prediction of the alloy. The large scale scatter in the elongation to failure data is in fact due to the influence of the solidification microstructure on this property.
Therefore the hardness and tensile tests have highlighted that specimens cut from a single casting, nominally subjected to the same heat treatment except for the pre-aging time (not usually considered in the industrial practice), can display a wide range of different mechanical properties with an obvious negative effect on the design stage of the component production. In addition, large differences in the minimum and maximum values of tensile strength and elongation to failure, due to the different solidification conditions that take place in the casting, suggest that the microstructure should be considered as input variable in the prediction of mechanical properties.

Tab. 2 Results of the tensile and hardness tests carried out on specimens extracted from two cylinder heads and subjected to different pre-aging times. The last raw (reporting min and max values for all the tested specimens) shows the great variation of properties achievable from two nominally identical castings.

pre-aging, min	HB		YS, MPa		UTS,MPa		E%	
	min	max	min	max	min	max	min	max
0	111	116	254	266	297	333	1.5	9.3
10	103	114	227	266	285	325	3.9	8.4
20	106	110	234	259	272	328	1.5	12.9
30	100	111	216	256	262	315	2.2	5.6
45	95	103	199	223	252	289	2.6	8.2
60	96	101	203	214	248	296	1.9	13.2
120	93	103	193	210	243	295	1.9	14.2
Total range:	**93**	**116**	**193**	**266**	**243**	**333**	**1.5**	**14.2**

MICROSTRUCTURAL ANALYSIS

The microstructure of the alloy is typical of a hypoeutectic Al-Si alloy, with primary α-Al dendrites and eutectic Si particles distributed around the Al dendrites to form a cell pattern periodically repeated across the metallographic surface. However, as can be seen from the micrographs reported in Fig. 2-4 and from the digital IA measurements reported in Tab. 3, significant microstructural differences were observed between the samples extracted from different zones of the castings.
The SDAS ranged between a minimum value of about 25 μm (Fig. 2a) and a maximum value of about 70 μm (Fig. 2b) depending on the local solidification rate. In fact, as reported in [6], SDAS [μm], in the A356 alloy, can be computed as:

$$SDAS = 39.4R^{-0.317} \quad (1)$$

where $R=dT/dt$ [°C/s] is the mean cooling rate during solidification of the α-Al phase. High solidification rates, reached for example near the combustion chamber (Zone 2 in Fig. 1b), reduce SDAS and thus generally lead to an improvement of almost all the mechanical properties (yield and tensile strength, as well as elongation to failure and fatigue resistance) [9, 10, 12]. Higher values of SDAS were instead measured in the camshaft seat zones (Zone 1 in Fig. 1b) where a large and complex system of cores and feeders is present.
The grain size ranged between a minimum value of about 200 μm to a maximum of 500 μm. Representative optical micrographs of the samples, electrolytically etched and observed under polarised light, are shown in Fig. 3. The grains surrounded by the eutectic Si (dark in the micrographs) can be clearly seen. Due to the efficiency of Ti-B as a nucleation agent, a quite homogeneous distribution of the grain size in the casting was observed, with a weak relationship with the cooling rate.
Since they control the mechanisms of failure, size, morphology and distribution of the eutectic silicon particles are also important microstructural parameters in cast Al-Si alloys [9-13]. It is well known that unmodified eutectic silicon has an undesired needle-like morphology that acts as a stress concentrator, reducing strength and ductility. The eutectic silicon particles can be modified to obtain a rounded morphology through rapid solidification, chemical modification and thermal modification in the solid state [21-24].

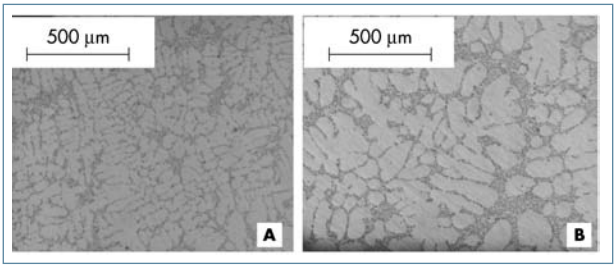

Fig. 2: Optical micrographs of the gravity die cast A356 alloy corresponding to zones with fine (a) and large (b) SDAS.

During the industrial production of these cylinder heads, a target value of 150 ppm (weight %) of Sr is introduced into the melt to obtain a finer and rounded eutectic silicon. The microstructural analyses, carried out on specimens cut from different zones of the cast, showed a different degree of eutectic Si modification partially depending on the cooling rate. As reported in [12, 22, 23], by increasing the solidification rate, the size and the aspect ratio of the eutectic silicon particles decrease (Fig. 4a). On the contrary, in zones where the cooling rates are lower, the eutectic Si particles appear larger and less modified, with a more lamellar morphology (Fig. 4b).
We measured defects content (gas pores and shrinkage cavities) using SEM on fracture surface of the tensile specimens (Fig. 5a) and using OM on some section of the casting (Fig. 1d). The results of the IA on the fracture surfaces (Tab. 3 and Fig. 5b) highlighted the very low level of porosity in this complex cast component. The percentage area fraction of the casting defects ranged from 0% to 4.2% for all the specimens except for one (extracted from a peripheral zone of the casting) where the presence of a cold-shut (Fig. 5a) and a total

Tab. 3 Results of the IA measurements carried out on the metallographic specimens and on the fracture surface of the 50 tensile specimens extracted from the cylinder head.

	Min	Max	Average	St. Dev.
SDAS, μm	25	70	50	13
d, μm	205	501	339	66
A, μm^2	8	19	13	2
AR	1.04	1.80	1.53	0.11
CS%	88.75	100	98	1.84

amount of defect of about 12.25% were observed.
IA on the four sections analysed using OM showed a maximum value of percentage area fraction of defects of about 2%, confirming the initial hypothesis that in a tensile specimen the fracture surface is the one with the highest content of defects.
The extremely poor content of defects measured using both OM and SEM analysis, indicated the high quality of the design of the bottom-gated and top-fed running system of this extremely complex casting.

CORRELATION ANALYSIS

Tab. 4 depicts the previously described correlation matrix. Note that only absolute values of the Pearson's coefficient were considered relevant in our analysis. YS is not significantly affected by the solidification microstructure while it is just depending on the alloy hardness. A hardness increase from 95 to 115 HB leads to a corresponding increase of the YS from about 200 to 260 MPa. As widely reported [25-27], the relationship between hardness and 0.2% proof strength of heat treatable aluminium alloys is mainly related to the strengthening effect of the Mg2Si precipitates induced by the T6 heat treatment. This kind of precipitates are in fact finely dispersed in the α-Al matrix, hindering the dislocations motion and therefore limiting the plastic deformation of the alloy. In this mechanism, microstructural parameters as SDAS play a minor role, for example promoting or inhibiting the diffusion of strengthening alloying elements during solution. A linear single variable (hardness) equation for 0.2% proof strength prediction was so chosen:

$$YS = 3.419 * HB - 127.6 \quad R^2 = 0.910 \quad (2)$$

The average error between the predicted YS values and the experimental ones (Fig. 6) was only 2.3% (about 5 MPa), while the maximum error was about 7%.

Tab. 4 also shows that, unlike the YS, the UTS and the E% were found to depend on the solidification microstructure. Hardness, SDAS, percentage cross section and area of eutectic silicon particle are the most affective parameters on UTS. As reported in [10], these microstructural parameters can influence the mechanical behaviour of the material. Crack nucleation and propagation occur in fact at discontinuities of the matrix (such as solidification defects and eutectic silicon particles) and are faster the larger the size of these discontinuities is. By considering the data reported in Tab. 2, we measured the maximum values of UTS for low SDAS values. A decrease of SDAS from 55 μm to 35 μm leads to an increase of UTS of about 30 MPa. The area of eutectic silicon and area fraction of defects registered a similar behavior: the higher the parameter the lower the property.
Based on the previously reported findings, an empirical equation (3) to predict the UTS taking into account hardness (HB), secondary dendrite arm spacing (SDAS) and percentage cross section (CS%) of tensile specimen was proposed:

$$UTS = 0.183 \cdot CS\%^{0} \cdot 803 \cdot SDAS^{-0,121} * HB^{0} \cdot 888 \quad R^2 = 0.899 \quad (3)$$

The average error between the predicted UTS values and the experimental ones (Fig. 7) was only 2.1% (about 5 MPa), while the maximum error was about 6%. From a practical point of view this model easily allows us to know the local UTS of the material also where tensile specimen cannot be extracted from the casting. Moreover, since hardness, SDAS and solidification defect content can be predicted by casting simulation software [28-30], it seems clear how this model could be applied in a co-engineered design approach.
Referring to equation (3), since solidification defects act as stress raisers (leading to an earlier fatigue crack nucleation) and higher hardness values are related to a more effective age hardening, positive exponents are needed for both percentage cross section and Brinell hardness. On the contrary, for SDAS, a negative exponent is needed, since a finer microstructure generally leads to higher mechanical properties [9-13].
The same considerations can also be made for the predictive equation of elongation to failure, reported below:

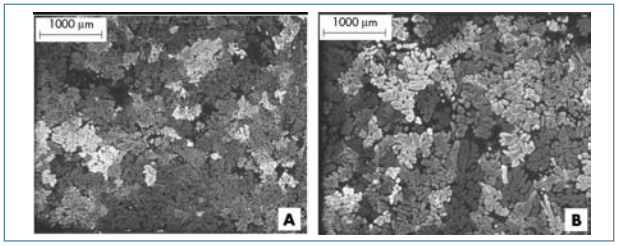

Fig. 3: Optical micrographs, under polarised light, of the gravity die cast A356 alloy, representative of zones with fine (a) and large (b) grain size.

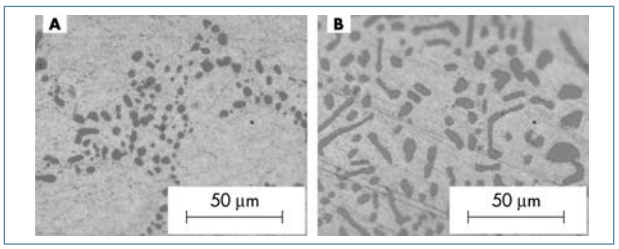

Fig. 4: Optical micrographs showing well modified (a) and partially modified (b) eutectic Si particles, corresponding to combustion chamber (high cooling rate) and camshaft seat zones (lower cooling rates), respectively.

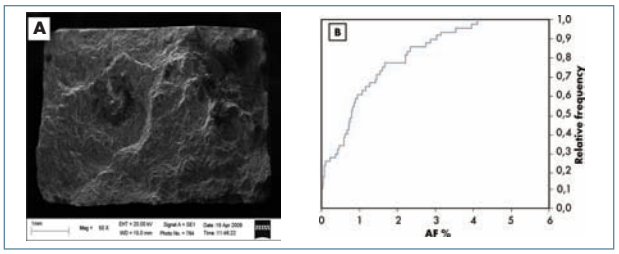

Fig. 5: Low magnification SEM micrograph of the fracture surface of the tensile specimen with the highest area fraction (12.25%) of solidifications defects (a) and the cumulative distribution of the percentage area fraction of defects (AF%) on the fracture surfaces of the tensile specimens.

Tab. 4 Correlation matrix (α = 0.05) for the tensile properties and microstructural parameters of the gravity die cast A356 alloy; in bold font > 0,4.

	YS	UTS	E%	HB	SDAS	d	A	AR	CS%
YS	1.000	0.836	0.005	0.956	-0.391	-0.323	-0.325	-0.316	-0.049
UTS	**0.836**	1.000	**0.518**	**0.833**	-0.706	-0.266	-0.675	-0.309	**0.527**
E%	0.005	**0.518**	1.000	**0.541**	-0.674	-0.314	-0.733	-0.316	**0.487**
HB	**0.956**	**0.833**	**0.541**	1.000	-0.379	-0.396	-0.306	-0.359	-0.013
SDAS	-0.391	-0.706	-0.674	-0.379	1.000	**0.573**	**0.712**	**0.548**	-0.150
d	-0.323	-0.266	-0.314	-0.396	**0.573**	1.000	**0.521**	**0.566**	0.059
A	-0.325	-0.675	-0.733	-0.306	**0.712**	**0.521**	1.000	**0.750**	-0.351
AR	-0.316	-0.309	-0.316	-0.359	**0.548**	**0.566**	**0.750**	1.000	-0.124
CS%	-0.049	**0.527**	**0.487**	-0.013	-0.150	0.059	-0.351	-0.124	1.000

$$E\% = 5074.8 * CS\%^{2} \cdot 951 \cdot SDAS^{-1.239} * HB^{-2.857} \cdot A^{-0.957}$$
$$R^2 = 0.813 \qquad (4)$$

It is worth noting that, despite the deep metallographic and fractographic analyses carried out in this study, the proposed model error when predicting the elongation to failure is significant (Fig. 8). A 20% average error between the predicted E% values and the experimental ones was in fact measured with peaks of about 80%. This large scatter between measured and calculated values is probably due to morphology and location of the solidification defects in the tensile specimen or to the size and distribution of Mg_2Si strengthening precipitates. Analysis on the latter should be carried out using TEM. A deeper analysis can be performed to evaluate the influence of these parameters on the elongation to failure. However the impossibility to determine them through casting simulation software has led us to neglect them in the present study.

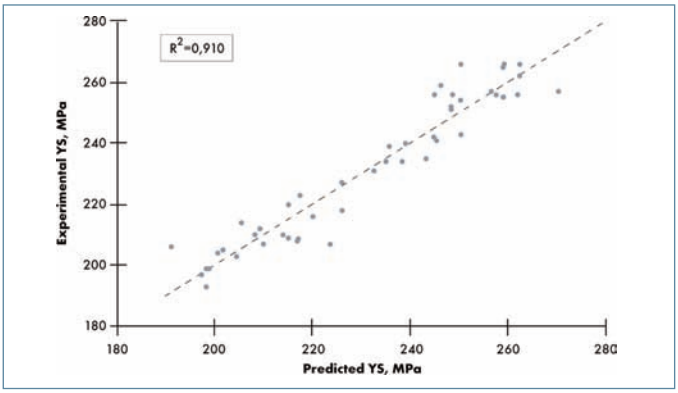

Fig. 6: Relationship between predicted (Eq. (2)) and experimental 0,2% proof strength.

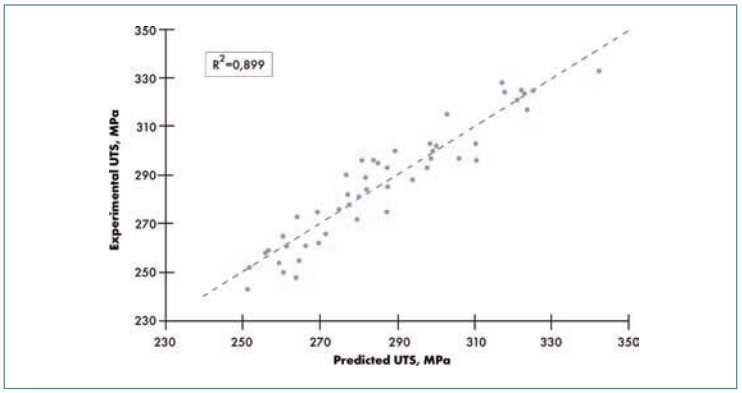

Fig. 7: Relationship between predicted (Eq. (3)) and experimental ultimate tensile strength.

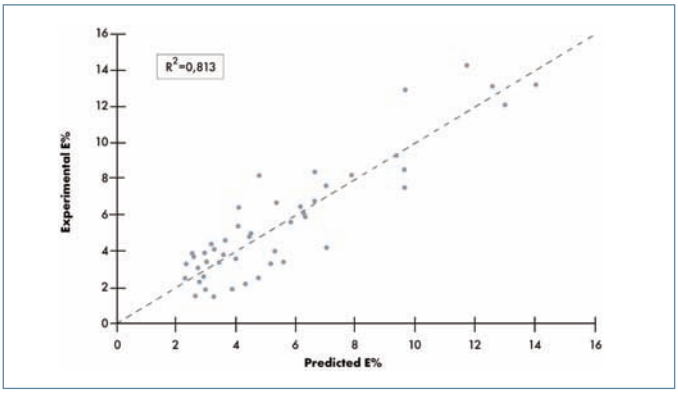

Fig. 8: Relationship between predicted (Eq. (4)) and experimental elongation to failure.

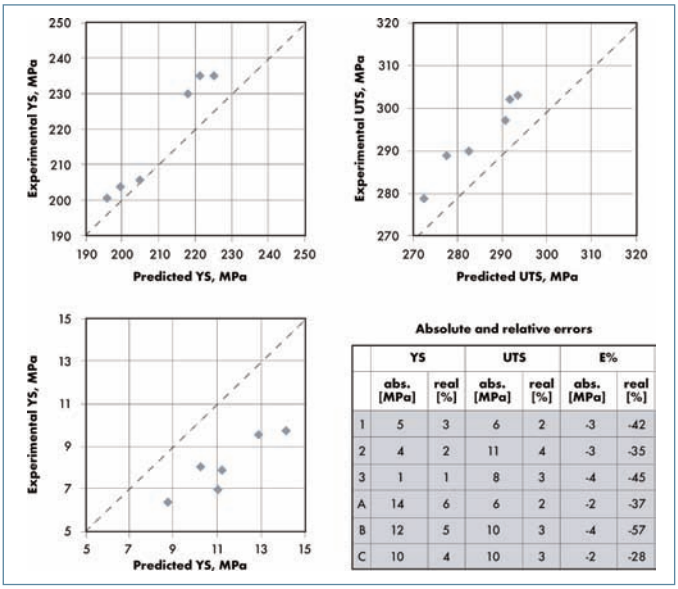

Absolute and relative errors

	YS		UTS		E%	
	abs. [MPa]	real [%]	abs. [MPa]	real [%]	abs. [MPa]	real [%]
1	5	3	6	2	-3	-42
2	4	2	11	4	-3	-35
3	1	1	8	3	-4	-45
A	14	6	6	2	-2	-37
B	12	5	10	3	-4	-57
C	10	4	10	3	-2	-28

Fig. 9: Predicted (Equations (2), (3) and (4)) and measured mechanical properties on tensile specimens extracted from two different batch production cylinder heads.

The data reported in Fig. 9 suggest that the predicted values are sufficiently close to the experimental one. The empirical models give the 0,2% proof strength and ultimate tensile strength of the alloy with a maximum error (underestimation) of 6%. On the contrary the predicted elongation to failure leads to overestimate the actual elongation to failure of the alloy of an average value of 40%. It is also worth noting that, despite the percentage error, the predicted values follow the increasing/decreasing patterns of the mechanical properties.

In order to clearly highlight the potential of the models, especially when used in combination with simulation software that can return good prediction of SDAS, defects content and hardness [28-30], we realised a map (Fig. 10) of the mechanical properties of the casting, by using the microstructural parameter measured on a section of the cylinder head (Fig. 1d).

On the contrary, the input variables of equation (4) can be simply evaluated with direct measurements or via simulation, except for the mean value of eutectic silicon area (A). This parameter ranges between 8 μm^2 and 16 μm^2 in the entire casting and is related with SDAS. Finer values of SDAS (<=45μm) lead to a mean value of about 10 μm^2 while larger values of SDAS (>45μm) lead to a mean value of 14 μm^2. This behaviour suggests that we could use equation (4) introducing pre-defined values of A according to the SDAS distribution in the casting.

VALIDATION AND APPLICATION OF THE MODELS

To verify the predictive models efficacy, we extracted six specimens from two different batch production cylinder heads. All the input variables of the empirical models for the six specimens have been evaluated (Tab. 5) and the tensile tests were performed. Predicted and experimental values of the mechanical properties of the six specimens are reported in Fig. 9.

CONCLUSIONS

In this work we propose empirical equations to predict tensile behaviour of A356 T6 gravity die casting as a function of hardness and microstructural parameters.

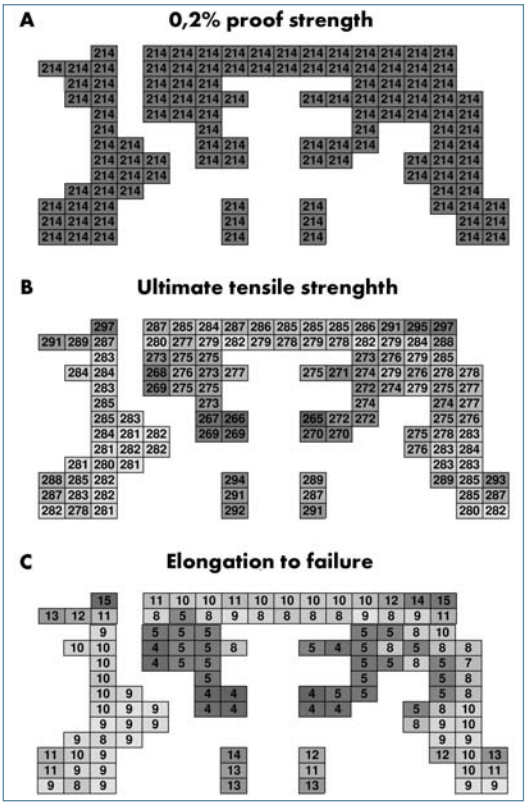

Fig. 10: Mechanical properties (YS (a), UTS (b) and E%) maps of a section (Fig. 1d) of the cylinder head, evaluated by introducing in equations (2), (3) and (4) the microstructural parameters (SDAS, CS%, A) measured on the metallographic specimens and a constant Brinell hardness value of 100.

- 0.2% proof strength can be predicted as a linear function of the hardness alloy. The mean error in the property prediction on the specimens extracted from industrial castings was 4% of the actual measured value.
- The ultimate tensile strength of the alloy was found to depend on SDAS, defects content and hardness. The mean error in the property prediction on the specimens extracted from industrial castings was 3% of the actual measured value.
- The elongation to failure of the alloy was found to depend on SDAS, defects content, hardness and eutectic silicon size. The mean error in the property prediction on the specimens extracted from industrial castings was 40% (overestimation) of the actual measured value.
- The shape of eutectic silicon and the grain size were not important parameter for the prediction of any of the tensile properties.
- The high error in the prediction of elongation to failure of the alloy might be related to the variable that were not considered in this study such as position and shape of casting defects, size and distribution of strengthening precipitates (Mg_2Si).
- The good results obtained suggest that the proposed model could be applied to the modern casting simulation software to obtain a mesh/map of mechanical properties that could be given as input to structural simulation software just during the component design phase.

Tab. 5 Hardness and microstructural parameters measured on tensile specimens extracted from two different batch production cylinder heads.

Cylinder Head	Specimen	HB	A [μm²]	SDAS [μm]	CS%
382	1	95	11	35	99.79
382	2	96	10	33	99.92
382	3	97	9	32	99.88
292	A	102	11	36	99.85
292	B	101	10	33	100.00
292	C	103	9	36	99.78

ACKNOWLEGMENTS

The author wish to acknowledge Ferrari SpA involved in the FAR research project "Design and development of mechanical components in aluminium alloys for engine applications with high performance and reliability under thermomechanical fatigue conditions", financially supported by the Italian Ministry of Education, University and Scientific Research. Many thanks are also due to prof. Lorella Ceschini and to prof. Alessandro Morri, for help, guidance and support in these two years of research.

REFERENCES

[1] J. A. Francis, G.M. Delphine Cantin, Mater. Sci. Eng. A, 2005.
[2] L. Ceschini, Al. Morri, An. Morri, A. Gamberini, S. Messieri, Mater. Des., 2009.
[3] A. K. Jha *, K. Sreekumar, Eng. Fail. Anal., 2009.
[4] J. Linder, M. Axelsson, H. Nilsson; Int. J. Fatigue, 2006.
[5] Q.G. Wang, D. Apelian, D.A. Lados, J. Light Metals , 2001, pp. 73-84.
[6] Q. G. Wang, D. Apelian, D. A. Lados, J. Lights Metals, 2001, pp.85-97.
[7] C.H. Càrceres, Scripta Mater., 1995.
[8] M. Tiryakioglu, J. Campbell, J.T.Staley, Scripta Mater., 2003.
[9] Q. G. Wang, C. H. Cáceres; Mater. Sci. Eng. A, 1998.
[10] Q.G. Wang, Metall Mater. Trans. A, 2003.
[11] C.H. Càceres, C.J. Davidson, J.R. Griffiths, Mater. Sci. Eng. A,1995.
[12] S. G. Shabestari, F. Shahri, J. Mat. Sci., 2004.
[13] E. Ogris, A. Wahlen, H. Lüchinger, P.J. Uggowitzer, J. Light Metals 2002.
[14] ASTM E 10 - 08 Standard Test Method for Brinell Hardness of Metallic Materials1
[15] UNI EN 10002-1:2004 Metallic materials - Tensile testing - Part 1: Method of test at ambient temperature.
[16] ASTM E3 polishing
[17] ASTM E 883 electrolytic etching
[18] ASTM E112-96 (2004) Standard Test Methods for Determining Average Grain Size
[19] N. R. Draper, H. Smith, Applied Regression Analysis, 1981, New York: John Wiley.
[20] S. Shivkumar, C. Keller, D. Apelian, AFS Trans. 1990.
[21] S.S. Sreeja Kumari, R.M. Pillai, T.P.D. Rajan, B.C.Pai, Mater. Sci. Eng. A 2007.
[22] M.M. Makhlouf, ASM Handbook ASM International, 2008.
[23] Guthy, Degree of Master of Science in Materials Science and Engineering at WPI, 2002
[24] S.K. Chaudhury, D. Apelian, Metall. Mater. Trans. A, 2006.
[25] P.A. Rometsch, G.B. Schaffer, Mater. Sci. Eng. A, 2002.
[26] M. Tiryakiglu, J. Campbell, J. T. Staley, Mater. Sci. Eng. A, 2003.
[27] S-W Han, K. Katsumata, S. Kumai, A. Sato, Mater. Sci. Eng. A 2002.
[28] S. Seifeddine, M. Wéssen, I. L. Svensson, Met. Sci. Tech., 2006.
[29] G. O. Verran, R. P. K. Mendes, M. A. Rossi, J. Mat. Proc. Tech., 2006.
[30] O. R. Myhr, Ø. Grong and S. J. Andersen, Acta mater. 2001.